Molecular dynamics simulations of the Mg^{2+}-stabilized Na^{+}- beta ''-alumina

1995 J. Phys.: Condens. Matter 7 2949

(http://iopscience.iop.org/0953-8984/7/15/003)

J. Phys.: Condens. Matter 7 (1995) 2949–2968. Printed in the UK

Molecular dynamics simulations of the Mg^{2+}-stabilized Na^+-β''-alumina

Bjørn Hafskjold and Xiaoyun Li†

Department of Physical Chemistry, University of Trondheim, The Norwegian Institute of Technology, N-7034 Trondheim, Norway

Received 29 June 1994, in final form 6 January 1995

Abstract. Ion transport mechanisms in Mg^{2+}-stabilized Na^+-β''-alumina were investigated by molecular dynamics simulations. Two compositions, different Mg^{2+} distributions, and different system sizes were used in the temperature range from 200 K to 1700 K. The trajectory plots of Na^+ ions and the Na^+–Na^+ radial distribution function demonstrated the formation of a vacancy superlattice at low temperature. The stability of the superlattice was found to depend crucially on the Mg^{2+} distribution. The ionic motions in the Na^+-β''-alumina were found to be highly correlated.

The sodium tracer self-diffusion coefficient and zero-frequency ionic conductivity were found to depend strongly on the Mg^{2+} distribution. This explains why the conductivity depends on the thermal history of Na^+-β''-alumina samples. The simulations show that the electrical conductivity can be increased by one order of magnitude at room temperature if the Mg^{2+} ions occupy optimal sites. The activation energy for Na^+ transport was shown not to be a static single-ion energy barrier, but it is numerically close to the pseudo-potential energy difference along conduction paths at high temperature. Correlated ionic motion was suggested to be the main reason for the very low activation energy in Na^+-β''-alumina.

1. Introduction

The Mg^{2+}-stabilized Na^+-β''-alumina is a very important solid electrolyte, which can be used in high energy-density batteries, e.g. Na/S batteries. Substantial efforts have been made in studying the properties of the material in the last two decades (Vashishta *et al* 1979, Poulsen *et al* 1985, Takahashi 1989).

Na^+-β''-alumina prepared under normal conditions is non-stoichiometric, and has the general formula $Na_{1+x}Mg_xAl_{11-x}O_{17}$, with $x \approx \frac{2}{3}$ in most cases. The main features of the electric conductivity of Na^+-β''-alumina are as follows. (i) The logarithm of the conductivity is a non-linear function of the inverse temperature, i.e. it shows a non-Arrhenius behaviour. (ii) It depends strongly on the preparation conditions of the material. For instance, the conductivity of a quenched single Na^+-β''-alumina crystal is four times higher than that of an unquenched crystal at room temperature (Davies *et al* 1986). (iii) The activation energy is 0.03–0.36 eV, which is very low compared to normal values for other fast ion conductors.

A theoretical study of Na^+-β''-alumina is essential in order to understand its properties. The molecular dynamics (MD) simulation method is chosen in this study because it allows us to investigate the detailed dynamics of the material at the molecular level.

The stoichiometric formula of Na^+-β''-alumina is $Na_2O{\cdot}MgO{\cdot}5Al_2O_3$, whose symmetry is rhombohedral with space group $R\bar{3}m$. The cell parameters are $a = b = 5.614$ Å and

† Current address: SINTEF Industrial Mathematics, N-7034 Trondheim, Norway.

0953-8984/95/152949+20$19.50

$c = 33.85$ Å at ambient temperature. The unit cell of Na^+-β''-alumina is composed of three spinel blocks separated by conduction slabs in which fast Na^+ transport can take place (see figure 1). In the spinel blocks, oxide ions form a cubic close-packed structure (thick lines labelled A, B, and C in figure 1(*a*)) with tetrahedral and octahedral aluminum sites. The oxide ions in the conduction slabs (the column oxygens, O_c^{2-}) are loosely packed (thick lines labelled A′, B′, and C′ in figure 1(*a*)). The sodium sites (tetrahedrally coordinated and crystallographically equivalent) lie alternately above and below the column oxygen layers and form a hexagonal honeycomb network in the conduction slab (figure 1(*b*)). In the non-stoichiometric material, about one-sixth of the Na^+ sites are vacant, and conduction occurs along the quasi-two-dimensional conduction slabs.

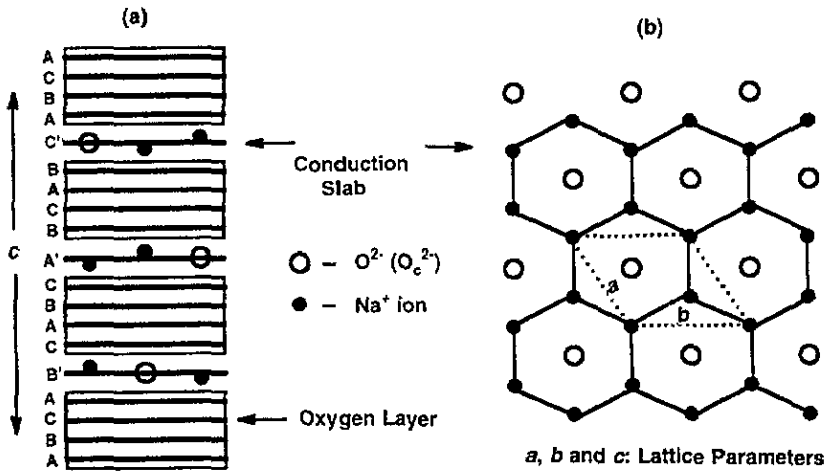

Figure 1. A schematic illustration of Na^+-β''-alumina. (*a*) The x–z projection. The conduction slabs are separated by spinel blocks. (*b*) The x–y projection of a conduction slab.

Figure 2 illustrates the profile of one-third of the x–z projection of the Na^+-β''-alumina unit cell. The Al^{3+} ions in the middle of the spinel block have two types of crystallographic sites. One type is octahedrally coordinated, termed the Al(4) site; this is located in the exact central plane in each spinel block. The other type is tetrahedrally coordinated, termed the Al(2) site. Alternate Al(2) sites lie slightly above and below the central Al(4) plane, and they are referred to as $Al(2)^a$ and $Al(2)^b$, respectively, in this study.

According to Roth *et al* (1976), the magnesium ions preferentially replace the tetrahedrally coordinated aluminum ions in the middle of the spinel blocks (i.e. the Al(2) sites). They also found that the sodium content in the conduction slabs varies with the magnesium content according to the composition formula $Na_{1+x}Mg_xAl_{11-x}O_{17}$, which was first suggested by Bettman and Peters (1969).

Extensive experimental and theoretical studies on Na^+-β''-alumina have led to the discovery that the sodium vacancies are ordered in superlattices at low temperatures, which has been related to the non-Arrhenius behaviour of the ionic conductivity (Collin *et al* 1979, Farrington and Briant 1979). Furthermore, magnesium ions are also found to have some kind of ordering, which in turn has been suggested to influence the electrical conductivity (Aldén *et al* 1986, Davies *et al* 1986).

Early MD simulations on the Na^+-β''-alumina revealed the Na^+ ion correlation (Wolf *et al* 1984) and the formation of a 2D superlattice of Na^+ ions in the conduction slab (Zendejas

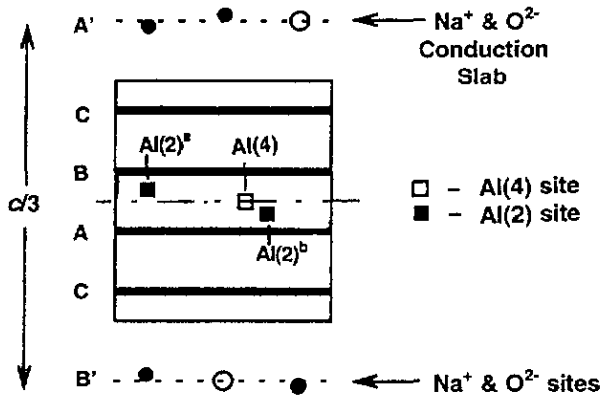

Figure 2. An illustration of aluminum sites Al(2) and Al(4) in the middle of the spinel block in Na^+-β''-alumina. The thick lines represent the close-packed oxygen layers.

and Thomas 1988). Comprehensive MD studies of large simulation cells were conducted by Smith and Gillan (1991, 1992), who showed the existence of the sodium vacancy superlattices for $x = \frac{2}{3}$ and $\frac{3}{4}$, and found that the symmetry of the vacancy superlattice is composition dependent. The temperature dependent conductivity data, converted from the simulated tracer self-diffusion coefficients, agreed with the well known non-Arrhenius behaviour of the sodium conductivity.

Some problems remain unsolved, however. What is the interplay between the formation of the vacancy superlattice, the ordering of the Mg^{2+} ions, and the non-Arrhenius behaviour of the ionic conductivity? Regarding the low activation energy for sodium transport in the Na^+-β''-alumina, is there any special effect that contributes in addition to the structural feature of the material?

In the present work, we have studied the vacancy ordering, the sodium diffusion coefficient, and the frequency-dependent conductivity with respect to the Mg^{2+} distribution in the material (see also the thesis of Li (1993)). In section 2, we describe the simulated systems, the parameters used, and the various conditions applied in this study. The vacancy correlation is discussed in section 3 on the basis of the trajectory plot and the radial distribution function. In section 4, the sodium diffusion coefficient and conductivity are discussed in detail. The activation energy for Na^+ transport is analysed and discussed in section 5. The conclusions from the present work are given in section 6.

2. Simulated systems

The interionic potentials used in the present study have the Born–Mayer–Huggins form:

$$V_{ij}(r) = Z_i Z_j e^2/4\pi\varepsilon_0 r + A_{ij}\exp(-r/\rho_{ij}) - C_{ij}/r^6. \tag{1}$$

This potential model was first used in the simulation of Na^+-β''-alumina by Wolf *et al* (1984). The material is assumed to be fully ionic, with charge valences of $Z_i = 3$, 2, 1, and -2 for Al, Mg, Na, and O, respectively. The potential parameters A_{ij}, ρ_{ij}, and C_{ij} for the different ion pairs are those derived empirically by Walker and Catlow (1982) and Catlow *et al* (1976) from studies of β-alumina and MgO (see table 1). This potential model has

Table 1. Potential parameters for the Na^+-β''-alumina system. The sources are: WC, Walker and Catlow (1982) and C, Catlow *et al* (1976).

Interaction	A_{ij} (eV)	ρ_{ij} (Å)	C_{ij} (eV Å^6)	Source
O^{2-}–O^{2-}	22 764.0	0.149 00	27.88	WC
O^{2-}–Na^+	1 226.8	0.306 5	0.0	WC
O^{2-}–Mg^{2+}	1 152.0	0.306 5	0.0	C
O^{2-}–Al^{3+}	1 460.3	0.299 12	0.0	WC
Na^+–Na^+	9 597.4	0.167 89	0.0	WC
Na^+–Al^{3+}	15 240.7	0.146 2	0.0	WC
Na^+–Mg^{2+}	0.0	N/A	0.0	WC
Al^{3+}–Al^{3+}	0.0	N/A	0.0	WC
Al^{3+}–Mg^{2+}	0.0	N/A	0.0	WC
Mg^{2+}–Mg^{2+}	0.0	N/A	0.0	WC

been shown to reproduce adequately several properties of Na^+-β''-alumina (Wolf *et al* 1984, Zendejas and Thomas 1988, Smith and Gillan 1991, 1992).

Two compositions, $x = \frac{2}{3}$ and $\frac{3}{4}$, were simulated. The corresponding Na^+ vacancy fractions are $\frac{1}{6}$ and $\frac{1}{8}$, respectively. In the stoichiometric form (i.e. $x = 1$ in $Na_{1+x}Mg_xAl_{11-x}O_{17}$), there are in total 90 ions in each unit cell, including six Na^+ ions. In most of the simulations, a $3a \times 4b \times 1c$ simulation box (mainly for composition $x = \frac{2}{3}$) and a $4a \times 4b \times 1c$ simulation box (for composition $x = \frac{3}{4}$) were used, where a, b, and c are the lattice constants in the hexagonal coordinate system. The non-stoichiometric 12-cell and 16-cell simulation boxes contained 1068 and 1428 ions, respectively. Some simulations were carried out in a larger simulation box, with dimensions $6a \times 6b \times 1c$, containing 36 unit cells, and with particle numbers 3204 and 3213 for $x = \frac{2}{3}$ and $x = \frac{3}{4}$, respectively.

In Na^+-β''-alumina, Mg^{2+} ions are introduced to substitute the Al^{3+} ions in the middle of the spinel blocks in order to balance the charge of sodium ions in the conduction slabs. To study the effect of different Mg^{2+} ion distributions, Al^{3+} ions at different sites were replaced by Mg^{2+} ions in the present study. The detailed Al^{3+} site locations in the middle of the spinel blocks are shown in figure 2. Three kinds of Mg^{2+} ion substitution were investigated.

(i) Mg^{2+} ions randomly substitute some Al^{3+} ions at the tetrahedral Al(2)^a sites, which leads to a completely unsymmetrical charge distribution with respect to the central plane of the spinel blocks. This kind of Mg^{2+} ion location is denoted by Mg(t1) in this study.

(ii) Mg^{2+} ions substitute both Al(2)^a and Al(2)^b atoms. A symmetrical charge distribution along the z-direction in the middle of the spinel blocks is achieved when there are equal numbers of Mg^{2+} ions at Al(2)^a and Al(2)^b sites. This position of Mg^{2+} ions is denoted Mg(t22). Under this constraint, the Mg^{2+} ions are randomly distributed among the available tetrahedral Al(2) sites.

(iii) Mg^{2+} ions substitute half the Al^{3+} ions at the octahedral Al(4) sites. This type of Mg^{2+} ion location also leads to a symmetrical charge distribution and is named Mg(o). The Mg(o) positions are randomly distributed among the Al(4) sites.

The number of Mg^{2+} ion substitutions depends on the sodium concentration (x in the composition formula).

Two sets of lattice parameters were used in the simulation, as follows.

(i) Lattice parameters $a = b = 5.614$ Å and $c = 33.85$ Å were used in all the simulations of the $x = \frac{3}{4}$ systems at all temperatures.

(ii) Based on a constant ratio c/a, the lattice parameters were adjusted at each temperature so that the simulation system had approximately zero pressure. In the text below, $a^{(t)}_{P\approx 0}$ and $a^{(o)}_{P\approx 0}$ are used to represent the sets of simulated lattice parameters for tetrahedral and octahedral locations of magnesium ions, respectively. These sets of lattice parameters were employed for $x = \frac{2}{3}$ systems ($N = 1068$ and 3204).

In our simulations, the atom coordinates were, for simplicity in calculating the forces, set in an orthogonal system. The sodium vacancies in each conduction slab were assigned randomly at the start, and high-temperature simulations were always carried out first so that the spontaneous development of the vacancy superlattice could be observed.

The Verlet neighbour list method (Allen and Tildesley 1987), the Beeman algorithm (Beeman 1976), and the Ewald method for calculating the Coulomb interactions (Fincham 1982) were applied. The timestep was $\Delta t = 5 \times 10^{-15}$ s in most of the simulations. The potential cut-off distance $R_{cut} = 6$ Å for short range interactions and for the real part of the Ewald sum.

3. Correlation of vacancies

3.1. Trajectory plots

Since Na^+-β''-alumina is a quasi-2D conductor, the projection of the Na^+ trajectories on the x–y plane is very illustrative in understanding the characteristics of the diffusive motion. Figure 3 shows that column O^{2-} ions vibrate around their ideal sites at both high (1000 K) and low (200 K) temperatures. By contrast, the Na^+ ions diffuse through the conduction slab. At high temperature, all the Na^+ ions are equivalent and there are no obvious vacant sites in the conduction slab, irrespective of the Mg^{2+} ion distribution. At low temperatures, the Na^+ diffusion is slow. In figure 3(b), an $a\sqrt{3} \times a\sqrt{3}$ vacancy superlattice can be observed (a is the lattice constant). Na^+ ions near vacancies relax towards them, which causes an average displacement of Na^+ ions from their ideal sites by about 0.78 Å. Na^+ ions that are not vacancy neighbours are, however, quite inactive, and they mainly vibrate around the ideal sites.

The Na^+ trajectories are quite different for symmetrical and unsymmetrical Mg^{2+} distributions at low temperature (200 K). When comparing figure 3(b) and (c), corresponding to unsymmetrical (Mg(t1)) and symmetrical (Mg(o)) Mg^{2+} distributions, respectively, it is obvious that the Na^+ ions in the latter case are much more active than those in the former. In figure 3(c), the Na^+ ions diffuse so rapidly that it is difficult to identify the vacancy superlattice from trajectories of the same time span (20 ps). However, trajectory plots of shorter time spans for the Mg(o) distribution at 200 K show that the vacancy superlattice is still formed, but it is rapidly deformed and reformed again. The same effect was observed for $N = 1428$ (i.e. composition $x = \frac{3}{4}$), except that the geometry of the vacancy superlattice changed to $2a \times 2a$.

Simulations of the large systems (36 unit cells) could not, however, show the stable existence of the $2a \times 2a$ superlattice at $x = \frac{3}{4}$, though an $a\sqrt{3} \times a\sqrt{3}$ superlattice is reproduced for $x = \frac{2}{3}$ (Li 1993). This result at $x = \frac{3}{4}$ disagrees with the simulation results obtained by Smith and Gillan (1991, 1992); more work is needed for the $x = \frac{3}{4}$ system to clarify the reason for this.

The trajectory plots suggest that the Mg^{2+} distribution in the middle of the spinel blocks plays a central role in determining the stability of the vacancy superlattice and the conductivity at low temperatures. The unsymmetrical distribution of Mg^{2+} ions makes the

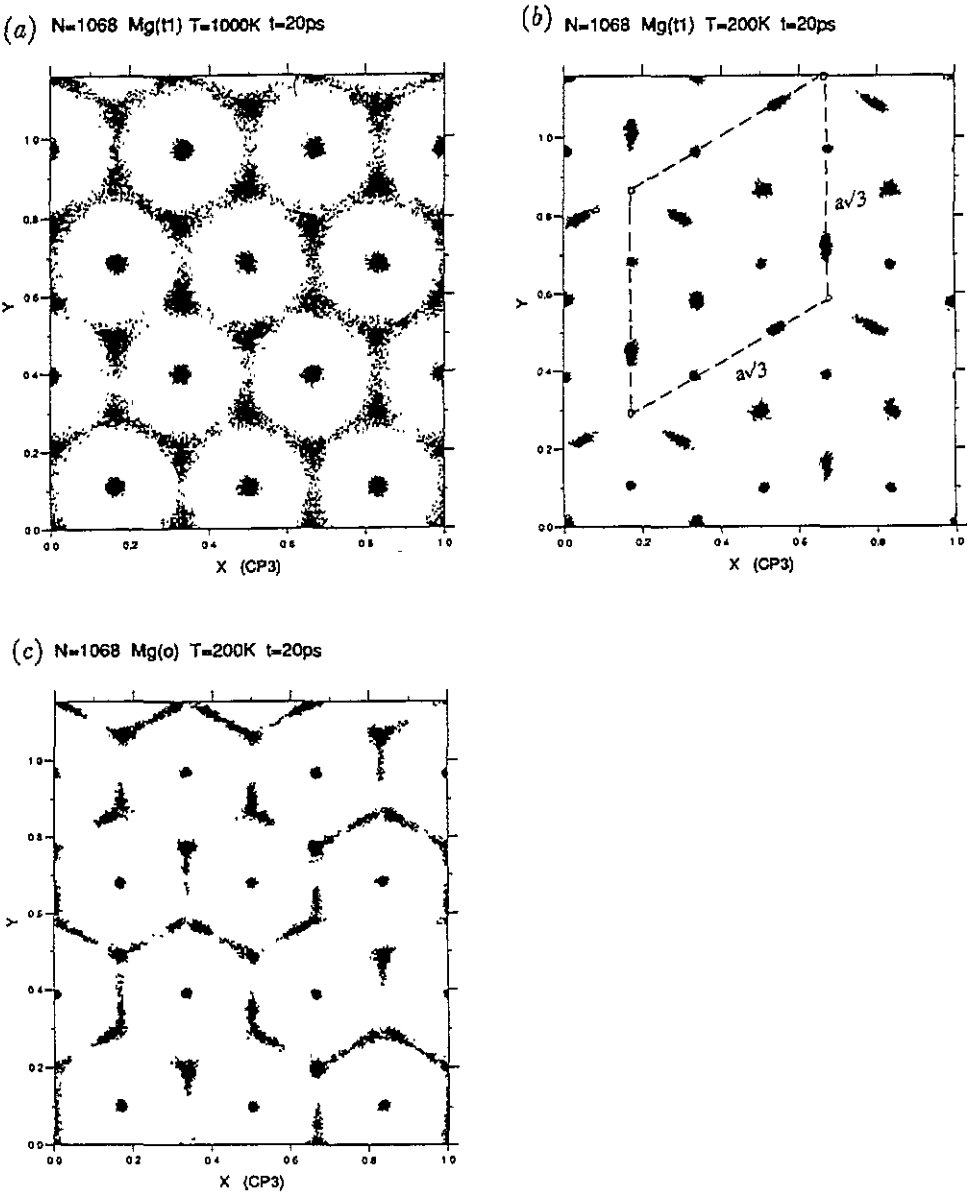

Figure 3. Trajectory plots of Na^+ and O^{2-} in the conduction slabs for the $N = 1068$ ($x = \frac{2}{3}$) systems. Plots (*a*) and (*b*) are based on unsymmetrical distribution of magnesium ions Mg(t1) at $T = 1000$ K and 200 K, respectively; and (*c*) is based on symmetrical distribution of magnesium ions Mg(o) at 200 K.

superlattice stable, while the symmetrical distribution of Mg^{2+} ions destabilizes the vacancy superlattice. This observation will be further discussed in subsections 4.1 and 4.2.

3.2. The Na^+–Na^+ radial distribution function

The behaviour of sodium ions in the conduction slab can also be illustrated by the radial distribution function of Na^+ ions. Figure 4 shows $g(r)$ versus r at 200 K and 500 K for

the $N = 1068$ ($x = \frac{2}{3}$) system. The Mg^{2+} ions were at Mg(t1) positions in this case. As expected, when the temperature increases, the first peak is reduced in height and broadened as a result of the structural disordering of Na^+ ions. At $r \approx 4.3$ Å, which corresponds to the average distance between the relaxed Na^+ ions, the $g(r)$ curve at 500 K is rather smooth, while the 200 K curve shows a shoulder at this distance. This result agrees with the earlier MD observations (Wolf *et al* 1984, Smith and Gillan 1992).

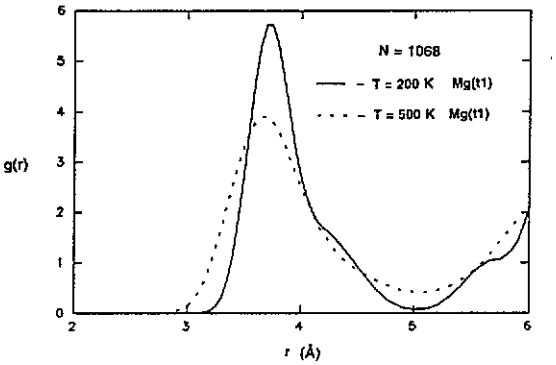

Figure 4. The radial distribution function of Na^+ ions in the $N = 1068$ ($x = \frac{2}{3}$) and Mg(t1) system.

The distribution of Mg^{2+} ions in the middle of the spinel blocks influences the radial distribution function as well as the trajectory plots. In figure 5, the curve at 200 K has a broadened first peak with reduced height when Mg^{2+} ions are symmetrically distributed (Mg(o)) as compared with the unsymmetrical distribution (Mg(t1)). In fact, the shoulder at $r \approx 4.3$ Å is hardly visible for the Mg(o) distribution, which agrees with the trajectory plot observation.

4. Sodium ion transport

4.1. The sodium diffusion coefficient

The Na^+ self diffusion coefficient, D^t, was computed from the 2D mean square displacement (MSD) by the Einstein relation:

$$\langle \Delta r_\parallel(t)^2 \rangle = B_\parallel + 4D_\parallel^t|t|. \tag{2}$$

Here, $B_\parallel$ is a constant and subscript $\parallel$ represents the direction parallel to the conduction slabs. There is no diffusion perpendicular to the conduction slabs. For simplicity, we will omit the subscript from the text below.

Na^+ diffusion coefficients with different Mg^{2+} ion distributions are given in tables 2 and 3 for the $x = \frac{2}{3}$ and $x = \frac{3}{4}$ systems, respectively. The data are also plotted in figure 6(*a*) and (*b*), respectively. The simulation results by Smith and Gillan (1992) at the same compositions are also shown (dashed line). These plots show that the diffusion coefficients depend crucially on the location of Mg^{2+} ions at low temperatures. The influence of the Mg^{2+} ion distribution also depends on the composition. At composition $x = \frac{2}{3}$ (with higher

Table 2. Sodium diffusion coefficients D^t calculated by the MSD method at composition $x = \frac{2}{3}$ with different Mg^{2+} ion distributions. $N = 1068$.

$N = 1068$ Mg(t1) $a_{p\approx 0}^{(t)}$		$N = 1068$ Mg(t22) $a_{p\approx 0}^{(t)}$		$N = 1068$ Mg(o) $a_{p\approx 0}^{(o)}$	
T (K)	D^t (10^{-9} m^2 s^{-1})	T (K)	D^t (10^{-9} m^2 s^{-1})	T (K)	D^t (10^{-9} m^2 s^{-1})
201.48 ± 0.05	0.0000 ± 0.0002	199.92 ± 0.04	0.09 ± 0.03	200.42 ± 0.08	0.13 ± 0.02
300.54 ± 0.06	0.04 ± 0.02	299.91 ± 0.07	0.44 ± 0.04	302.14 ± 0.08	0.38 ± 0.05
503.7 ± 0.1	1.00 ± 0.07	499.1 ± 0.1	1.34 ± 0.09	502.8 ± 0.2	1.53 ± 0.07
703.4 ± 0.2	1.9 ± 0.2	698.4 ± 0.1	2.9 ± 0.1	699.6 ± 0.3	3.1 ± 0.1
1000.4 ± 0.2	4.3 ± 0.2	1004.4 ± 0.2	4.6 ± 0.1	905.6 ± 0.5	4.1 ± 0.1
1503.2 ± 0.3	7.2 ± 0.2	1504.1 ± 0.5	8.0 ± 0.2	997.2 ± 0.2	4.9 ± 0.1
1702.6 ± 0.8	8.6 ± 0.3			1099.1 ± 0.3	5.6 ± 0.1
				1715.4 ± 0.7	9.3 ± 0.2

Table 3. Sodium diffusion coefficients D^t calculated by the MSD method at composition $x = \frac{3}{4}$ with different Mg^{2+} ion distributions. $N = 1428$ and $a = 5.614$ Å.

$N = 1428$ Mg(t1)		$N = 1428$ Mg(o)	
T (K)	D^t (10^{-9} m^2 s^{-1})	T (K)	D^t (10^{-9} m^2 s^{-1})
204.28 ± 0.06	0.024 ± 0.005	203.27 ± 0.08	0.23 ± 0.02
305.36 ± 0.08	0.19 ± 0.03	305.7 ± 0.1	0.74 ± 0.04
504.4 ± 0.1	0.91 ± 0.04	502.83 ± 0.09	1.62 ± 0.08
704.8 ± 0.2	2.26 ± 0.06	706.6 ± 0.1	2.5 ± 0.1
1003.8 ± 0.2	3.57 ± 0.07	1006.4 ± 0.4	3.9 ± 0.2
1511.6 ± 0.5	6.0 ± 0.1	1514.6 ± 0.6	6.1 ± 0.1

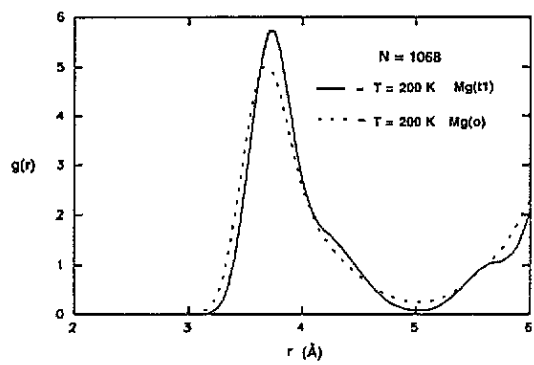

Figure 5. The radial distribution function with different Mg^{2+} ion distributions in $N = 1068$ Na^+-β''-alumina systems.

vacancy fraction), the effect is much stronger than at $x = \frac{3}{4}$. At both compositions, the D^t values are small when the Mg^{2+} ions are located at the unsymmetrical Mg(t1) sites. By contrast, the symmetrical Mg(t22) and Mg(o) distributions give high diffusion rates at low temperatures. The influence from the Mg^{2+} ion distribution becomes smaller when the temperature increases.

The difference between our results and those of Smith and Gillan may be explained by different Mg^{2+} distributions. Since the Mg^{2+} ion distribution in their simulations is unknown

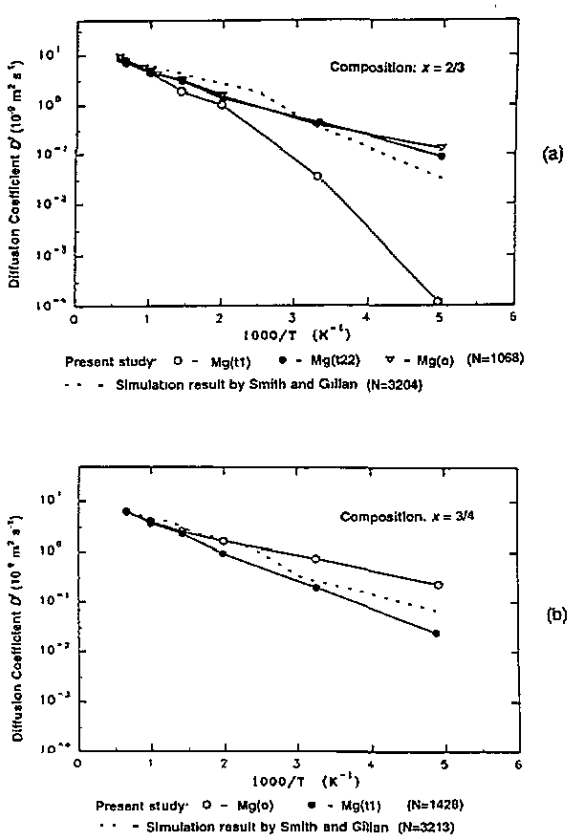

Figure 6. Sodium diffusion coefficients D^1 in Na^+-β''-alumina at compositions (*a*) $x = \frac{2}{3}$ and (*b*) $x = \frac{3}{4}$.

to us, it is difficult to make detailed comparison. The ionic conductivities computed by Smith and Gillan are much higher than the experimental data. From our simulation results, we suggest that this is explained by different Mg^{2+} distribution conditions between their simulations and real experiments.

Davies *et al* (1986) found that the conductivities of Na^+-β''-alumina samples are very different for the unquenched and quenched samples at temperatures below 473 K. Our diffusion coefficient results for the unsymmetrical and symmetrical Mg^{2+} ion distributions show similar temperature dependences as do the conductivities of the unquenched and quenched samples, respectively. Unfortunately, there is no directly measured Na^+ diffusion coefficient data available for single-crystalline Na^+-β''-alumina, thus it is impossible to make any direct comparison at this stage. It has to be pointed out that our Mg^{2+} ion distributions are two possibly extreme cases, while in real materials, the Mg^{2+} ion distribution would be expected to be somewhere in between.

Davies *et al* (1986) and Aldén *et al* (1986) supposed that quenched Na^+-β''-alumina samples have a higher degree of randomness in Mg^{2+} ion distribution than the unquenched samples. They attributed the thermal history effect on conductivity to the Mg^{2+}/Al^{3+} ordering in spinel blocks. Our simulation results with different Mg^{2+} ion locations strongly support their point of view.

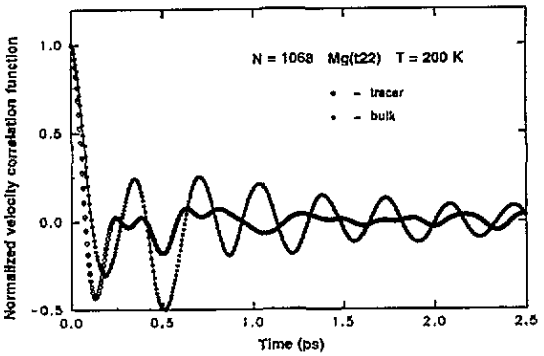

Figure 7. Self- and bulk VCFs at $x = \frac{2}{3}$, Mg(t22) distribution, and $T = 200$ K. The bulk VCF shows the largest oscillations.

4.2. Ionic conductivity

The frequency dependent ionic conductivity $\sigma(f)$ can be calculated by the Green–Kubo formula (Kubo 1957, 1966):

$$\sigma(f) = \frac{1}{z\Omega k_B T}\int_0^\infty \mathrm{d}t\, \mathrm{e}^{\mathrm{i}2\pi f t}\,\langle J_c(t)\cdot J_c(0)\rangle \tag{3}$$

where z is the dimensionality (equal to two in the present case), f is the frequency and Ω is the system volume. J_c is the fluctuating electrical current associated with the motion of ions. Suppose there is only one type of conducting ion, then J_c is just

$$J_c = Z\sum_{i=1}^{N}\nu_i \tag{4}$$

where Z is the ionic charge, N is the number of conducting ions, and ν_i is the velocity of ion i. The conductivity may also be related to the bulk diffusion coefficient, D^b, by

$$\sigma = (Z^2\rho/k_B T)D^b \tag{5}$$

where $\rho = N/\Omega$ is the number density of the conducting ions. Based on (3) and (4), the frequency-dependent tracer and bulk diffusion coefficients may be defined by

$$\begin{aligned} D^t(f) &= \frac{1}{zN}\int_0^\infty \mathrm{d}t\, \mathrm{e}^{\mathrm{i}2\pi f t}\left\langle \sum_{i=1}^{N}\nu_i(t)\cdot\nu_i(0)\right\rangle \\ D^b(f) &= \frac{1}{zN}\int_0^\infty \mathrm{d}t\, \mathrm{e}^{\mathrm{i}2\pi f t}\left\langle \sum_{i=1}^{N}\nu_i(t)\cdot\sum_{j=1}^{N}\nu_j(0)\right\rangle. \end{aligned} \tag{6}$$

The Haven ratio is defined as (Compaan and Haven 1956, Le Claire 1970)

$$H_R = \frac{D^t(0)}{D^b(0)} \tag{7}$$

and D^t is related to the DC conductivity $\sigma(0)$ by (Le Claire 1970, Murch 1982)

$$\sigma(0) = (Z^2\rho/k_BT)D^t(0)/H_R. \tag{8}$$

Figure 7 shows the velocity correlation functions (VCF) of Na^+ ions at 200 K with Mg(t22) location for $x = \frac{2}{3}$. The damped oscillatory feature of the velocity autocorrelation function is typical for diffusive motion of tracer ions in a fast ion conductor. The bulk velocity of Na^+ ions shows an oscillating feature, suggesting that the motions of the conducting ions are highly correlated.

The diffusion coefficients D^t and D^b were calculated at several temperatures, and the resulting Haven ratio is shown as a function of temperature in figure 8. Although these results may not be very accurate, it is still worthwhile to notice how its temperature dependence varies with the Mg^{2+} distribution and vacancy concentration. For instance, at 500 K, H_R is 50% higher for $x = \frac{3}{4}$ than for $x = \frac{2}{3}$ with the Mg(t1) positions, whereas the two compositions give almost the same H_R at 1500 K.

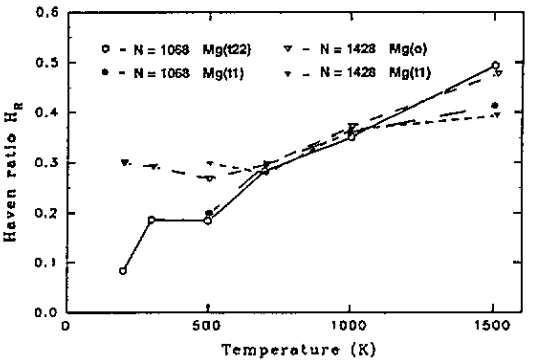

Figure 8. The Haven ratio of the simulated Na^+-β''-alumina systems.

Ormrod and Kirk (1977) have measured the Haven ratio for mixed Li_2O- and MgO-stabilized polycrystalline β''-alumina samples, and found values of H_R ranging between 0.18 and 0.15 in the temperature range from 368 K to 873 K. Miles *et al* (1972) measured H_R in several polycrystalline samples of β''-alumina and mixed ($\beta'' + \beta$)-alumina from 298 K to 873 K and found that it depended strongly on temperature for the β''-alumina sample. At 673 K, the H_R value is about $\frac{1}{3}$; it decreases to 0.14 at ambient temperature. However, since one cannot rule out the possibility of ion transport along grain boundaries in polycrystalline samples, the resulting H_R values cannot be regarded as representing the bulk property completely. It should also be mentioned that Kim *et al* (1979) and Chandrashekhar and Kim (1981) measured the DC conductivity for a Na^+-β-alumina single crystal and the tracer diffusion coefficient for the same crystal in a wide temperature range (from 194 K to 873 K). The H_R value was found to be 0.18 at the lowest temperature and 0.45 at the highest temperature. There is a striking discontinuity for the Haven ratio at about 500 K in their measurements. No measurements of H_R have to our knowledge been made for single β''-alumina crystals yet.

Since β-alumina and β''-alumina are structurally closely related materials, and considering the high sodium vacancy concentration in β-alumina, we suggest that the low H_R values at low temperatures are related to the correlated motions of ions. In fact, from

the definition of the Haven ratio, we find that a small H_R value corresponds to highly correlated velocities of different conducting ions, indicating that ions move in the same direction simultaneously. Thereby the temperature dependence of H_R can be understood as showing the degree of correlation among mobile ions in the conduction slabs. At low temperatures, the correlation effect is stronger at $x = \frac{2}{3}$ than at $x = \frac{3}{4}$.

Arrhenius plots of the DC conductivities, determined from (5) at compositions $x = \frac{2}{3}$ and $x = \frac{3}{4}$, are shown in figure 9. In addition to the conductivity results from this study, the experimental data at composition $x \approx \frac{2}{3}$ of Davies *et al* (1986) are also presented. Once again, we see the different temperature dependences of the conductivities, depending on the Mg^{2+} distribution.

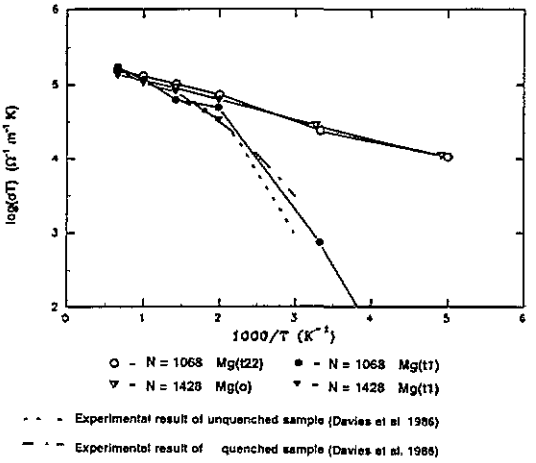

Figure 9. Arrhenius plots of the conductivities for the Na^+-β''-alumina systems at compositions $x = \frac{2}{3}$ ($N = 1068$) and $x = \frac{3}{4}$ ($N = 1428$).

Table 4. The activation energies for the simulated Na^+-β''-alumina systems at composition $x = \frac{2}{3}$ ($N = 1068$).

	$E_a^{diff.}$ (eV)		$E_a^{cond.}$ (eV)	
Mg^{2+} ion distribution	$T > 600$ K	$T < 400$ K	$T > 600$ K	$T < 400$ K
Unsymmetrical (Mg(t1))	0.13	0.26	0.09	0.28
Symmetrical (Mg(t22))	0.09	0.09	0.06	0.06

5. Activation energy and transport mechanisms

From the slopes of the Arrhenius plots, we can derive the activation energies for conduction and diffusion. Table 4 lists the activation energies obtained from the simulations of the $x = \frac{2}{3}$ ($N = 1068$) systems (i.e. from figures 6 and 9). Several observations can be made here.

(i) For systems with symmetrical Mg^{2+} distributions, there is essentially only one activation energy in the whole temperature range studied. By contrast, unsymmetrical Mg^{2+} distributions lead to different activation energies in the high and low temperature ranges.

(ii) The symmetrical Mg^{2+} distributions result in extremely low activation energies for conduction and diffusion.

(iii) As a trend, the activation energies for conduction are somewhat lower than the corresponding activation energies for diffusion. Recalling the low Haven ratio at low temperatures, we suggest that this is explained by the correlated ionic motion, which contributes more to the ionic conductivity than to the sodium tracer self-diffusion.

For experimental activation energies from conductivity measurements of single crystalline Na^+-β''-alumina, different preparation conditions often yield substantially different results. For the unquenched sample, Davies *et al* (1986) found 0.34 eV and 0.10 eV at low ($T < 400$ K) and high ($T > 600$ K) temperatures, respectively, but for the quenched sample, they found a linear Arrhenius plot and one activation energy, 0.165 eV, in the entire temperature range from 300 K to 1000 K. Briant and Farrington (1980) reported activation energies in the range from 0.20 to 0.31 below 400 K and from 0.09 to 0.12 above 600 K, depending on the crystal growth temperature. Table 4 shows that our simulated activation energies for conduction with the Mg(t1) distribution agree well with the activation energies measured in the high- and low-temperature regimes by the above authors.

There are two ways of interpreting the activation energy in the limit of dilute defect concentration, as (i) the single-ion energy barrier an atom experiences during a jump from one site to another or (ii) the energy difference between the activated state (a midway position of one ion between two normal sites) and the ground state (all atoms at their normal sites). The activation energy is in the second case related to the instantaneous potential energy change of the whole system.

To check these interpretations the energies and coordinates of ions in a conduction slab were recorded sequentially for a period of 10 ps, and jump events were identified. For the sake of illustration, we consider the $N = 1068$, Mg(t1), and $T = 300$ K system only. Figure 10(a) shows the displacements of a selected Na^+ ion from its initial position and from a nearest ideal Na site. This ion has a vacancy neighbour, which is why it never occupies an ideal lattice site. For example, during the period from 0 to 0.5 ps, the Na^+ ion made a jump, followed by an immediate return jump. Figure 10(b) shows the kinetic energy and potential energy of the same ion in the same time span. The kinetic energy is very small (< 0.2 eV) as compared to the magnitude of the fluctuation in the potential energy (~ 2 eV) of the ion. These values suggest that besides the contribution from kinetic energy, a jump process may be accomplished mainly by exchanging potential energy among ions. The potential energy change of a single ion during a jump is entirely overshadowed by the large fluctuations of the ion's potential energy. It is difficult to define the activation energy as a pure single-ion quantity from the figure.

The potential energy per Na^+ ion and per O_c^{2-} ion in the same conduction slab are plotted in figure 11(a). The potential energy per ion in the conduction slab and per ion in the whole system irrespective of ion type are shown in figure 11(b). The amplitude of the potential energy fluctuation per Na^+ ion in the conduction slab is much smaller than the potential energy fluctuation of the single Na^+ ion. The potential energy per Na^+ ion also shows some oscillatory behaviour, indicating the strong correlation among sodium ions. Furthermore, the motion of Na^+ ions is also correlated with the O_c^{2-} ions in the same conduction slab, which reduces the amplitude of the potential fluctuation in the conduction slab substantially.

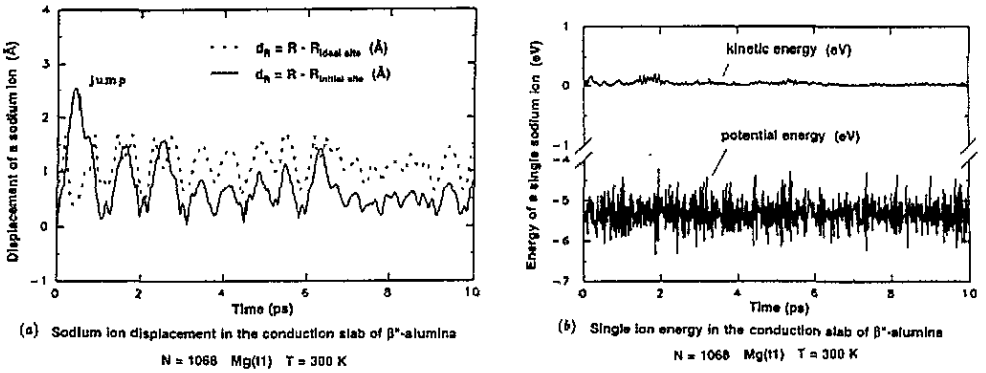

Figure 10. The displacement of a single sodium ion in the conduction slab and the ion's kinetic and potential energies. $N = 1068$, Mg(t1), $T = 300$ K, $t = 10$ ps.

The rest of the potential energy fluctuation in the conduction slab is absorbed by the spinel blocks. Fluctuations in the potential energy per ion for the whole system are not detectable as we can see in figure 11(b). The numerical value of the activation energy for diffusion cannot be determined from any quantity discussed above.

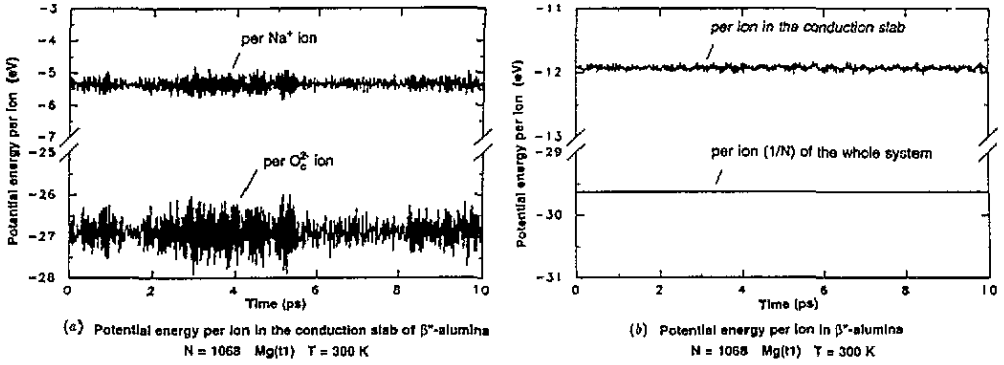

Figure 11. The potential energy per ion in the simulated Na^+-β''-alumina system at 300 K.

Similar potential energy analyses at higher temperatures show the same features. As a consequence, the observed activation energy from diffusion measurements will not be a single-ion energy barrier. The correlated motion of ions also causes difficulties in studying the activation energy as an instantaneous quantity in Na^+-β''-alumina.

The time-averaged particle density $\rho(\boldsymbol{r})$ was computed and related to the *pseudo-potential energy* (Zucker and Schultz 1982, Bachmann and Schultz 1984),

$$\rho(\boldsymbol{r}) \propto \exp\left(-V(\boldsymbol{r})/k_{\mathrm{B}}T\right). \tag{9}$$

The pseudo-potential energy is a composite potential energy that results from the superposed potentials of conducting ions in various possible neighbour configurations. In a structurally ordered system, each site is well defined and isolated, and the density map will be single

peaked at each site. The pseudo potential along a conduction path can be taken as the average potential energy of the conducting ions. Averaged over space and time, the difference between the potential maximum and minimum along the conduction paths is the average energy barrier that ions have to overcome in order to migrate through the system. If the transport mechanism does not change with increasing temperature, the pseudo-potential energy difference along a conduction path has been found to be temperature independent, and the numerical value of this pseudo-potential energy difference can be compared to the activation energy from conductivity measurements (see the article by Bachmann and Schultz (1984) and references therein).

When there are crystallographically inequivalent sites very close to each other, so-called split-atom positions, the density maps will contain the superposed information of these inequivalent sites. As a result of the split-atom positions, there will be a pseudo-potential minimum at each of them, and the pseudo potential along conduction paths will be very shallow at low temperatures. As the temperature increases, the split-atom positions gradually merge at one centre, and the density maps become sharply peaked. For split-atom positions, the pseudo-potential difference along conduction paths will typically increase with increasing temperature (Bachmann and Schultz 1984).

We have already seen from the trajectory plots that there are two kinds of sodium sites in Na^+-β''-alumina at low temperatures, namely the ideal hexagonal 6c sites where the unrelaxed Na^+ ions are located, and the 18h sites where Na^+ ions relax towards vacancies. Between any two ideal hexagonal sites (6c), there are two possible 18h sites, as illustrated in figure 12. An Na^+ ion can be at either a 6c or an 18h site depending on whether its neighbour 6c Na^+ sites are occupied or not at low temperatures.

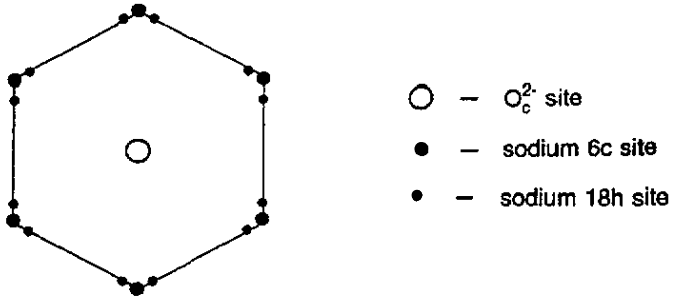

Figure 12. An illustration of Na^+ sites in Na^+-β''-alumina.

Figure 13(a) and (b) shows the density and the corresponding pseudo-potential energy, respectively, of Na^+ ions in the simulated $N = 1068$, Mg(o), and $T = 200$ K system. The split-sodium positions, 6c and 18h sites, are clearly seen. The pseudo-potential energy difference along the conduction paths is very small as shown in figure 13(b).

Figure 14(a) and (b) shows the density and the pseudo-potential energy, respecively, of Na^+ ions for the $N = 1068$, Mg(o), and $T = 1100$ K system. The density map at this temperature shows clearly the single-peaked 6c sodium sites, and no significant occupancy of the 18h sites is detected. An average value 0.12 eV for the potential energy difference along the conduction paths can be obtained from figure 14(b).

In table 5, we have listed the pseudo-potential energy differences, ΔV, averaged over all the conduction slabs at different temperatures for the $N = 1068$ and Mg(o) system. At low

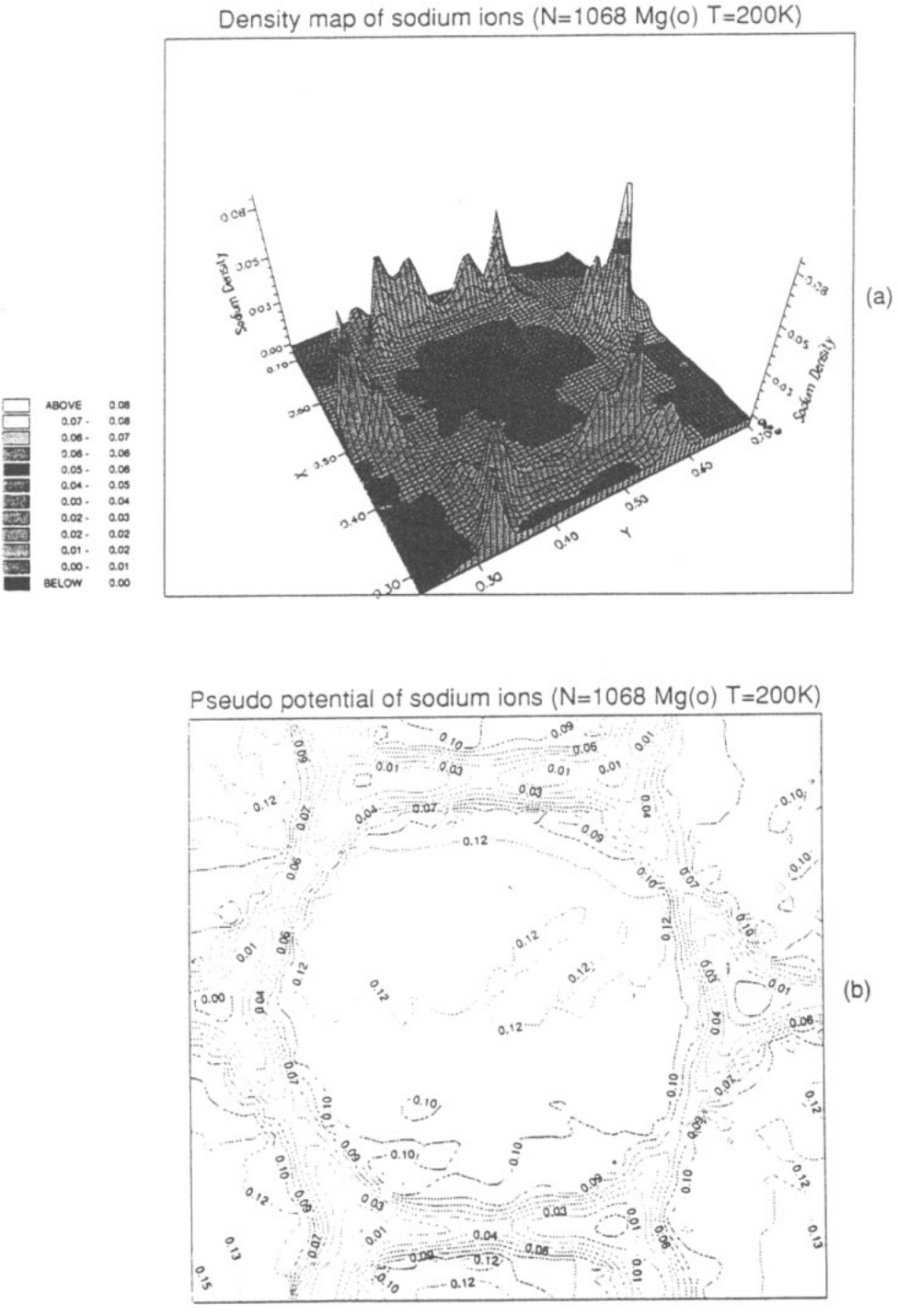

Figure 13. The density map and the pseudo-potential energy of sodium ions in the simulated $N = 1068$ and Mg(o) system. $T = 200$ K.

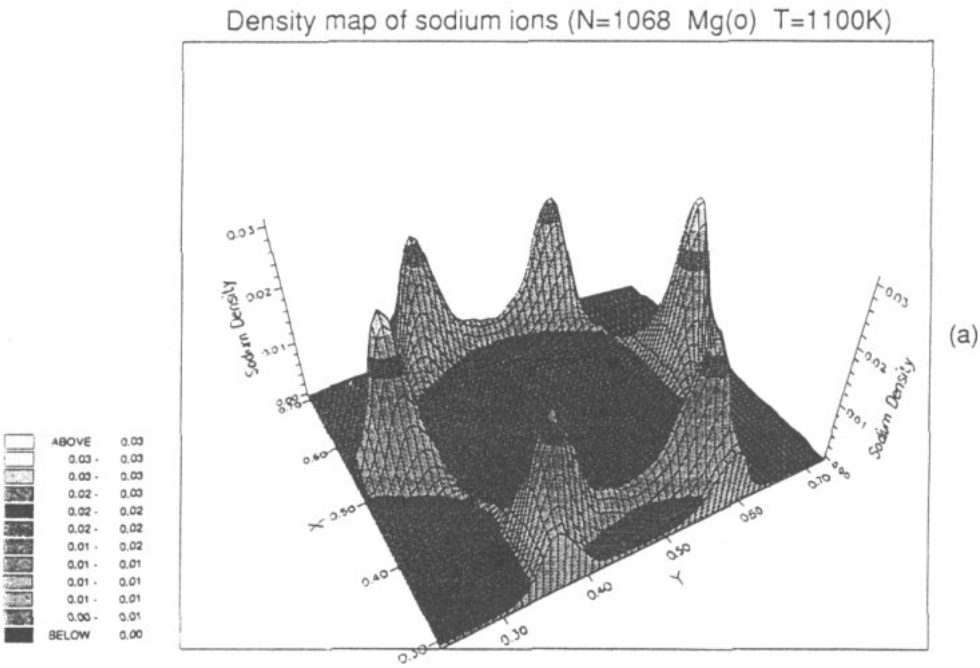

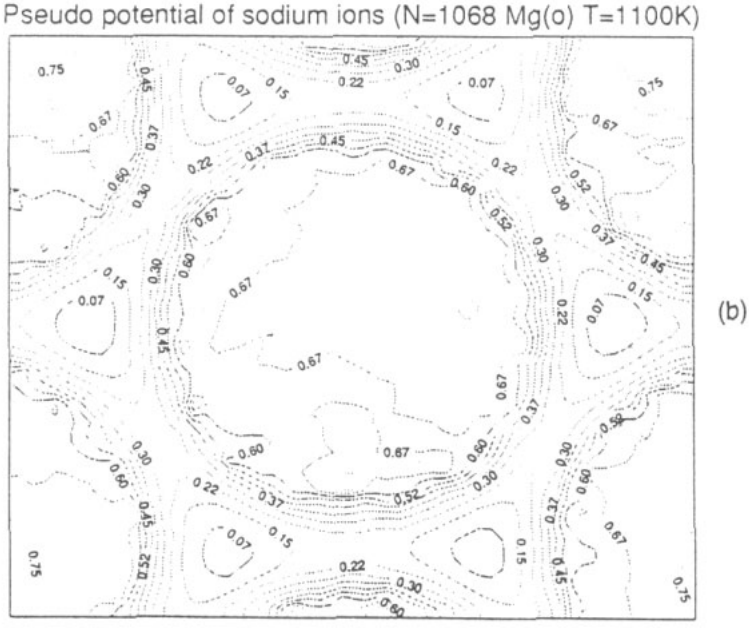

Figure 14. The density map and the pseudo-potential energy of sodium ions in the simulated $N = 1068$ and Mg(o) system. $T = 1100$ K.

temperatures, with split-sodium positions, very small ΔV values were obtained. The ΔV increases with increasing temperature. When the temperature further increases, ΔV becomes temperature independent, indicating an ordered unit cell structure. We can thus compare the high-temperature ΔV with the average activation energy for conduction. The approximate value, 0.12 eV, at elevated temperatures is in fact not very far from the activation energies in the high-temperature regime from conductivity measurements (Briant and Farrington 1980, Davies *et al* 1986), but the agreement with the activation energy derived from our VCF calculations is not very good (see table 4 for the Mg(t22) distribution).

Table 5. Pseudo-potential energy differences along Na^+ conduction paths in the $N = 1068$ and Mg(o) Na^+-β''-alumina simulation system.

Temperature (K)	200	300	500	700	900	1000	1100
ΔV (eV)	0.03	0.08	0.09	0.12	0.12–0.14	0.12–0.13	0.11–0.14

Considering all these results from the present simulations, we suggest that the activation energy for sodium transport is determined by two separate effects. One is the interionic correlation in the conduction slabs, the other is the interaction between the mobile ions and the spinel block.

Now we can postulate the role of Mg^{2+} ion distribution and explain the conductivity behaviour in Na^+-β''-alumina as follows:

(i) *The unsymmetrical Mg^{2+} distribution.* The unsymmetrical Mg^{2+} ion distribution produces some deep potential wells in the conduction slabs and the Na^+ sites become energetically inequivalent. This makes some Na^+ ions more fixed at their lattice positions at low temperatures. Vacancy superlattices are formed such that the repulsion between vacancies is minimal. To destroy a vacancy superlattice and form a new one needs a lot of energy because some Na^+ ions are reluctant to leave their low-energy sites.

In this case, although the motions of ions are correlated in the conduction slabs, the static potential formed by the spinel blocks is also important in determining the overall activation energy for Na^+ transport. When the temperature is elevated, one observes the gradual disappearance of the vacancy ordering. The correlations of ions in the conduction slabs will dominate in determining the activation energy at high temperatures. This explains why a marked change in the activation energy for Na^+ ion transport can be observed when Mg^{2+} ions are unsymmetrically distributed.

(ii) *The symmetrical Mg^{2+} distribution.* A symmetrical distribution of Mg^{2+} ions levels out the potential paths in the conduction slabs and there is no energetic difference between the Na^+ sites. Since the vacancy superlattice configuration gives minimum repulsion between vacancies, the system will try to keep this kind of arrangement, but all the Na^+ sites are equally preferable for vacancies, and other Na^+ ions can easily exchange their positions with vacancies. What one can observe from the trajectory plot of a conduction slab is the frequent change of 'vacancy superlattice–reordering–new vacancy superlattice' states. Averaged over a long time, there is no preferred vacancy site in the conduction slab and a high diffusion rate is obtained even at low temperatures.

In this case, the static potential formed by the spinel blocks is rather weak. The interionic correlation in the conduction slabs dominates at all temperatures in determining the activation energy for Na^+ transport. In other words, there is eventually only one contribution to the activation energy at low and high temperatures. This argument is supported by the ideal Arrhenius behaviour of the Na^+ diffusion coefficients and conductivities from our simulations with symmetrical distributions of Mg^{2+} ions (i.e. Mg(t22) and Mg(o)).

6. Conclusions and suggestions

In the present study of Na^+-β''-alumina, we have shown that the stability of the vacancy superlattice in the conduction slabs depends crucially on the Mg^{2+} distribution in the spinel blocks. The interplay between the Mg^{2+} distribution and the temperature dependence of the conductivity or diffusion is also demonstrated clearly by the simulation results. For the two compositions studied, we found that the influence of Mg^{2+} ion distribution on ion transport is weaker at $x = \frac{3}{4}$ than at $x = \frac{2}{3}$ for the non-stoichiometric Na^+-β''-alumina ($Na_{1+x}Mg_xAl_{11-x}O_{17}$).

Unsymmetrical distribution of Mg^{2+} ions causes strong correlation of vacancies in the conduction slabs, and leads to low conductivities and low diffusion coefficients at low temperatures.

We suggest that the activation energy for Na^+ transport originates from two combined effects. One is the interionic correlation in the conduction slabs, the other is the interaction between the mobile ions and the spinel block. The strength of this interaction depends on the Mg^{2+} ion distribution, resulting in the different conductivity behaviour at different Mg^{2+} distributions. Highly correlated ionic motions in the conduction slab have been observed at both low and high temperatures from the potential energy analysis. These findings are also manifested by the extremely low Haven ratio at low temperatures and the oscillatory behaviour of the bulk velocity correlation function of Na^+ ions. The Haven ratio is found to depend on temperature and vacancy concentration. We suggest that the correlated motions of ions are responsible for the low activation energy in Na^+-β''-alumina.

Since the motions of ions in the conduction slabs are highly correlated, the activation energy for diffusion or conduction cannot be regarded as a single-ion energy barrier in Na^+-β''-alumina. The correlated motion also makes it difficult to interpret the activation energy as an instantaneous quantity of the whole system. Instead, it can be treated as a collective quantity.

At low temperatures, the Na^+ sites have split positions; the potential energy difference along conduction paths increases with increasing temperature, and the numerical value cannot be related to the activation energy. At high temperatures, the structure of the mobile ion sublattice is ordered in each unit cell; the potential energy difference along conduction paths is almost temperature independent, and the numerical value is comparable to the average activation energy.

Acknowledgments

We wish to thank Professor John Kincaid from The State University of New York at Stony Brook for many constructive discussions. The main FORTRAN code MDIONS was provided by Dr Fincham at the Computer Centre at University of Keele. Financial support for this work was provided by NAVF (The Norwegian Research Council for Science and Humanities, grant No 432.89/070) and an NTH (The Norwegian Institute of Technology) scholarship. NAVF has also supported this work through free CPU time on the Cray Y- MP supercomputer at RUNIT (Trondheim). Free computer time was also provided by the IBM cluster at USIT (University of Oslo).

References

Aldén M, Thomas J O and Davies P 1986 *Solid State Ionics* **18/19** 694–698

Allen M P and Tildesley D J 1987 *Computer Simulation of Liquids* (Oxford: Clarendon)
Bachmann R and Schultz H 1984 *Acta Crystallogr.* A **40** 668–75
Beeman D 1976 *J. Comput. Phys.* **20** 130–139
Bettman M and Peters C R 1969 *J. Phys. Chem.* **73** 1774–80
Briant J L and Farrington G C 1980 *J. Solid State Chem.* **33** 385–90
Catlow C R A, Faux I D and Norgett M J 1976 *J. Phys. C: Solid State Phys.* **9** 419–29
Chandrashekhar G V and Kim K K 1981 *Solid State Commun.* **37** 299–301
Collin G, Colomban Ph, Boilot J P and Comes R 1979 *Fast Ion Transport in Solids* ed P Vashishta, J N Mundy and G K Shenoy (Amsterdam: North-Holland) pp 309–14
Compaan K and Haven Y 1956 *Trans. Faraday Soc.* **52** 786–801, 1498–1508
Davies P K, Garzon F, Feist T and Katzan C M 1986 *Solid State Ion.* **18/19** 1120–8
Farrington G C and Briant J L 1979 in Fast Ion Transport in Solids ed P Vashishta, J N Mundy and G K Shenoy (Amsterdam: North-Holland) pp 395–400
Fincham D 1982 *Comput. Phys. Commun.* **25** 159–176, 177–9
Gillan M J *1989 Ionic Solids at High Temperatures* ed A M Stoneham (Singapore: World Scientific) pp 169–247
Kim K K, Mundy J N and Chen W K 1979 *J. Phys. Chem. Solids* **40** 743–755
Kubo R 1957 *J. Phys. Soc. Japan* **12** 570
—— 1966 *Rep. Prog. Phys.* **29** 255
Le Claire A D 1970 *Phys. Chem.—An Advanced Treatise Vol 10/Solid State* ed W Jost (New York: Academic) pp 261–329
Li X 1993 *Dr. Ing. Thesis* Norwegian Institute of Technology, University of Trondheim
Miles L J, Jones I W, Le Claire A D and Rowe A H 1972 *Electrochem. Soc. Extended Abstracts Spring Meeting (Houston, TX, 1972)* abstract **166** pp 425–6
Murch G E 1982 *Solid State Ion.* **7** 177–98
Ormrod S E and Kirk D L 1977 *J. Phys. D: Appl. Phys.* **10** 1497–507
Poulsen F W, Andersen N H, Clausen K, Skaarup S and Sørensen O T (ed) 1985 *Transport–Structure Relations in Fast Ion and Mixed Conductors, Proc. 6th Risø Int. Symp. on Metallurgical and Materials Science*
Roth W L, Reidinger F and Laplaca S 1976 *Superionic Conductors* ed G D Mahan and W L Roth (New York: Plenum) pp 223–41
Smith W and Gillan M J 1991 *Ber. Bunsenges. Phys. Chem.* **95** 967–71
—— 1992 *J. Phys.: Condensed Matter* **4** 3215–34
Takahashi T (ed) 1989 *High Conductivity Solid Ionic Conductors, Recent Trends and Applications* (Singapore: World Scientific)
Vashishta P, Mundy J N and Shenoy G K (ed) 1979 *Fast Ion Transport in Solids* (Amsterdam: North-Holland)
Walker J R and Catlow C R A 1982 *J. Phys. C: Solid State Phys.* **15** 6151–61
Wolf M L, Walker J R and Catlow C R A 1984 *Solid State Ion.* **13** 33–8
Zendejas M A and Thomas J O 1988 *Solid State Ion.* **28–30** 46–52
Zucker U H and Schultz H 1982 *Acta Crystallogr.* A **38** 563–8